Triaxiality in selenium-76

J. Henderson,[1,*] C. Y. Wu,[1] J. Ash,[2,3] B. A. Brown,[2,3] P. C. Bender,[4] R. Elder,[2,3] B. Elman,[2,3] A. Gade,[2,3] M. Grinder,[2,3] H. Iwasaki,[2,3] B. Longfellow,[2,3] T. Mijatović,[2] D. Rhodes,[2,3] M. Spieker,[2] and D. Weisshaar[2]

[1]*Lawrence Livermore National Laboratory, Livermore, California 94550, USA*

[2]*National Superconducting Cyclotron Laboratory, Michigan State University, East Lansing, Michigan 48824, USA*

[3]*Department of Physics and Astronomy, Michigan State University, East Lansing, Michigan 48824, USA*

[4]*Department of Physics and Applied Physics, University of Massachusetts Lowell, Lowell, Massachussetts 01854, USA*

(Received 23 January 2019; published 13 May 2019)

Background: Selenium and germanium nuclei are associated with both triaxiality and shape coexistence. The relative influence of these deformation effects on the low-lying nuclear structure remains the subject of much discussion with additional attention drawn to ^{76}Se and ^{76}Ge due to the potential for the observation of neutrinoless double-β decay.

Purpose: Experimental observables related to the deformation of ^{76}Se are lacking in precision. The purpose of the present paper is to provide electric quadrupole matrix elements with improved precision in order to determine the deformation of low-lying states in a model-independent manner.

Methods: Sub-barrier Coulomb excitation was employed at the reaccelerated beam facility of the National Superconducting Cyclotron Laboratory using the JANUS setup. Using this method nineteen $E2$ matrix elements were extracted.

Results: Extracted matrix elements agree within uncertainties with those in the literature but with improved precision. Through both a comparison with geometric models and a model-independent evaluation of $E2$ matrix elements using rotational invariants, the ground state of ^{76}Se is best described as having a significant triaxial component, but is not maximally triaxially deformed.

Conclusions: Selenium-76 exhibits a significant degree of triaxiality in its ground state. A detailed comparison with configuration-interaction calculations indicates that this can be well reproduced theoretically.

DOI: 10.1103/PhysRevC.99.054313

I. INTRODUCTION

Atomic nuclei exhibit the bulk property of deformation, commonly assuming nonspherical shapes far from nuclear magic numbers. It is becoming increasingly clear that axially symmetric prolate and oblate extremes of quadrupole deformation are not sufficient to describe many nuclei with triaxial components to the deformation often found to be significant. One area of the nuclear landscape where the role of axially asymmetric deformation has long been inferred to be important is the selenium germanium region. The low-lying γ band in these isotopes—associated with a triaxial vibrational mode—is indicative of this, whereas the staggering of the band members has been used to infer the rigidity of this triaxial deformation (see, e.g., Ref. [1]). More recently, comprehensive Coulomb excitation analyses using state-of-the-art γ-ray detection arrays have cemented this picture of triaxial deformation in, for example, ^{72}Ge [2].

Understanding the role of deformation in these isotopes is made a more pressing issue by its influence on the calculation of the nuclear matrix element for the hypothesized neutrinoless double-β decay process with ^{76}Ge being an excellent candidate for observation [3,4]. Differing ground-state deformations in the parent (^{76}Ge) and daughter (^{76}Se) nuclei result in a reduced spatial overlap between the initial- and the final-state configurations. Any reduction in overlap will inhibit the process as inferred more explicitly through theoretical calculations (see, e.g., Ref. [5]).

Reproducing the germanium selenium region microscopically provides a challenge for nuclear theory. The fpg shell itself is large, but small-amplitude excitations into the $2d_{5/2}$ orbital are known to play an important role in driving quadrupole deformation and are typically too computationally expensive to include in calculations. Over the past decade, however, Hamiltonians have been developed to tackle this region of the nuclear landscape with examples pertinent to this paper being the JUN45 [6] and the $jj44b$ (see Appendix A in Ref. [7]) interactions.

In order to provide a clearer picture of the role of deformation in the selenium isotopes, more extensive and precise experimental data are required. In particular, transition matrix elements connecting low-lying states are known to be sensitive to deformation effects and might be reproduced theoretically by, for example, shell-model calculations with the aforementioned interactions. Here, we present results from a sub-barrier Coulomb excitation measurement of ^{76}Se performed on a high-Z target to allow for multistep excitation. This methodology allows us access to multiple $E2$ matrix elements connecting low-lying states, improving precision over literature values. The new more precise results are then used to construct a series of rotationally invariant quantities related to

*henderson64@llnl.gov

the quadrupole deformation parameters of the nucleus, both with respect to the absolute magnitude of the ground-state deformation and its degree of triaxiality.

II. EXPERIMENTAL DETAILS

The present measurements were performed at the reaccelerated beam facility (ReA3 [9]) of the National Superconducting Cyclotron Laboratory (NSCL [10]). Stable ^{76}Se ions were injected into the NSCL's electron-beam ion trap [11] and charge bred prior to injection into the ReA accelerator chain. To enhance sensitivity to the nuclear matrix elements, ^{76}Se was delivered at two energies: 4.07 and 3.55 MeV/u, maintained for 24 and 72 h, respectively, and impinged upon an enriched 0.92-mg/cm^2-thick ^{208}Pb target. Mean on-target intensities were maintained at approximately 2×10^5 pps for the duration of the experiment. The beam energies corresponded to minimum impact parameters of 5 and 7.5 fm, 72% and 62% of the Coulomb barrier for the higher and lower energies, respectively. Scattered beam- and targetlike nuclei were detected in the JANUS setup for Coulomb excitation [12], consisting of a pair of S3-type annular silicon detectors located upstream and downstream of the target. The downstream and upstream target-silicon detector separations were measured to be 26 ± 1 and 34 ± 1 mm, respectively. Emitted γ rays were detected in the segmented germanium array (SeGA) [13], consisting of 16 32-fold segmented HPGe detectors. Data were extracted using a digital data-acquisition system, made up of 33 100-MHz (SeGA) and 8 250-MHz (silicon detectors) XIA Pixie-16 modules in a triggerless continuous-running mode. Events were constructed on the basis of the master clock and analyzed using the GRUTINIZER [14] software package, built in a ROOT framework [15]. The experimental setup was identical to that described in Ref. [16].

III. ANALYSIS

Silicon pixels were constructed from time- and energy-coincident ring and segment hits in the S3 detectors. Beamlike (^{76}Se) and targetlike (^{208}Pb) recoil loci were identifiable in the observed kinematics. γ rays detected in SeGA were Doppler corrected for ^{76}Se velocities event by event on the basis of the reaction kinematics and the beam- or targetlike nature of the detected particle. The transitions observed are summarized in Fig. 1. At both beam energies, targetlike events were excluded from the analysis at angles greater than 40° (rings 13 and above) to avoid biasing of the data due to dead-layer effects in the silicon detectors. Detections in the upstream detector were entirely excluded for the lower beam energy for the same reason. The observed particle energies are shown in Fig. 2 plotted against the downstream ring number. Clearly, beam- and targetlike loci are well separated. Low-level contamination from a lighter ion is seen at roughly the 1% level. This contamination does not impact the analysis of the experimental data presented below.

The beamlike locus in the downstream S3 detector was subdivided into six angular bins, each composed of four annular rings. In the case of the ^{208}Pb-gated kinematics, the

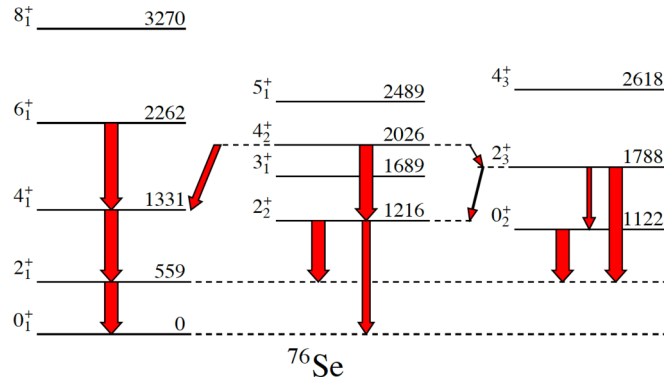

FIG. 1. Level scheme indicating the observed transitions. Note that the experiment is sensitive to unobserved transitions by including data from the literature, such as branching ratios. Arrow widths correspond to relative branching ratios [8].

data were subdivided into two angular bins containing six rings, corresponding to the 12 shallowest angle rings. Wider angle targetlike events were excluded because of the dead-layer effects discussed previously. The upstream detector was considered as a whole in the higher-energy experimental setting. Doppler-corrected γ-ray spectra were constructed from SeGA coincidences with these angular bins for both the high- and the low-energy portions of the experiment. The experimental data were thereby separated into 17 groups for Coulomb-excitation analysis. Example Doppler-corrected γ-ray spectra, corresponding to beam- and targetlike detections at the higher beam energy are shown in Fig. 3. The Doppler correction is superior for beamlike particle detection. In the case of targetlike detection, the beamlike particle is scattered at angles approaching 90° and, therefore, travels further in the target material, causing a broadening of the line shape. Figure 4 shows example Doppler-corrected γ rays detected

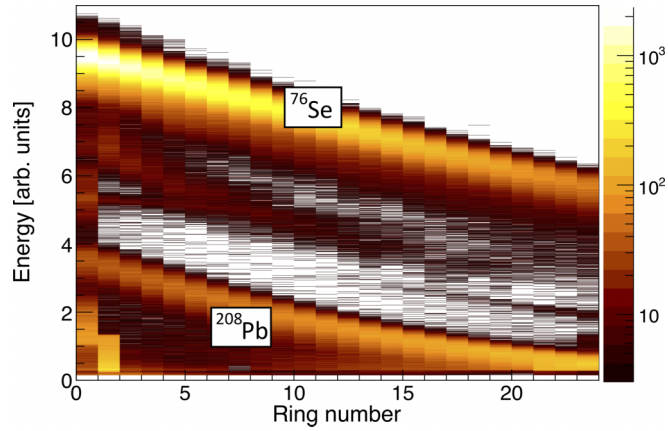

FIG. 2. Pixel energy in the downstream JANUS silicon detector plotted against ring number with smaller ring numbers corresponding to shallower angles. The data shown were acquired at a beam energy of 4.07 MeV/u. Dominant in the spectrum are the kinematic lines originating from the scatter of ^{76}Se and ^{208}Pb. Also seen is a lighter contaminant at approximately a 1% level. Note that bins with two or fewer counts are excluded from this figure to aid clarity.

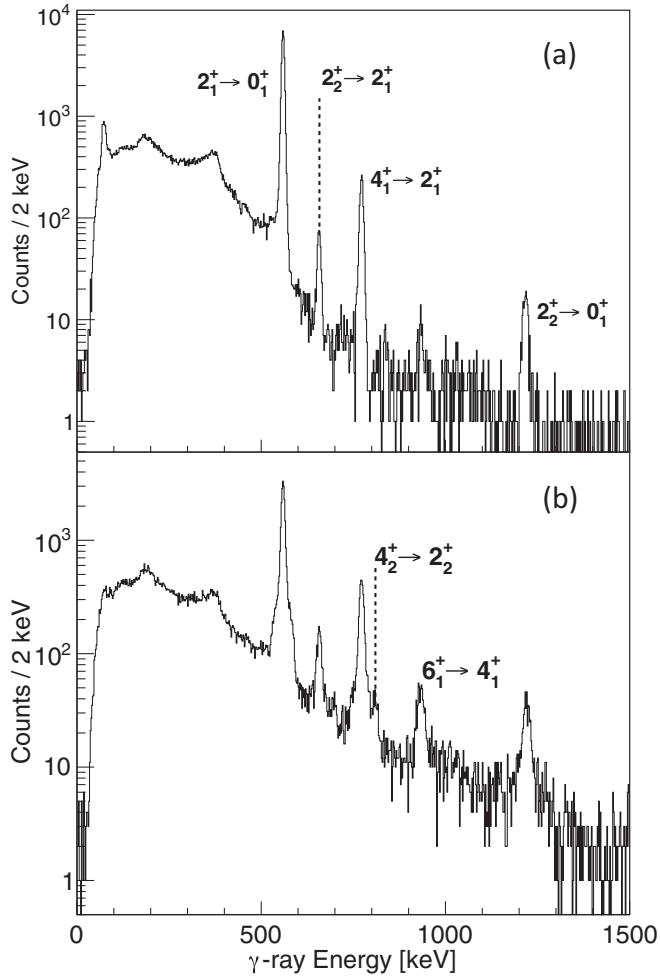

FIG. 3. Doppler-corrected γ rays coincident with the detection of a beamlike (top) and targetlike (bottom) particles in the downstream silicon detector at a beam energy of 4.07 MeV/u with the strongest transitions highlighted. The non-Gaussian shapes in coincidence with the detection of targetlike particles arise from the wide scattering angles of the beamlike particles in coincidence, resulting in them traversing a longer distance in the target material and inducing a line shape.

in coincidence with a particle in the upstream detector. This detection condition corresponds to a best-case scenario for Doppler correction. In the general case, multiplets, such as those shown in the bottom two panels of Fig. 4, were unresolvable.

The $0_2^+ \rightarrow 2_1^+$ and $2_1^+ \rightarrow 0_1^+$ transitions (bottom panel, Fig. 4) are separated by only 4 keV and, as such, cannot be resolved in coincidence with downstream detection due to the larger velocities. In order to enhance sensitivity both to the multistep excitation $0_1^+ \rightarrow 2_1^+ \rightarrow 0_2^+$ and to the quadrupole moment of the 2_1^+ state it is desirable to quantify the relative contributions to the combined peak around 560 keV. Utilizing the high efficiency of the SeGA array this was achieved using γ-γ coincidences. In order to use γ-γ coincidences, it is necessary to account for changes in detection efficiency as a result of the γ-γ angular distribution. This efficiency correction was determined empirically through comparison to cascades both

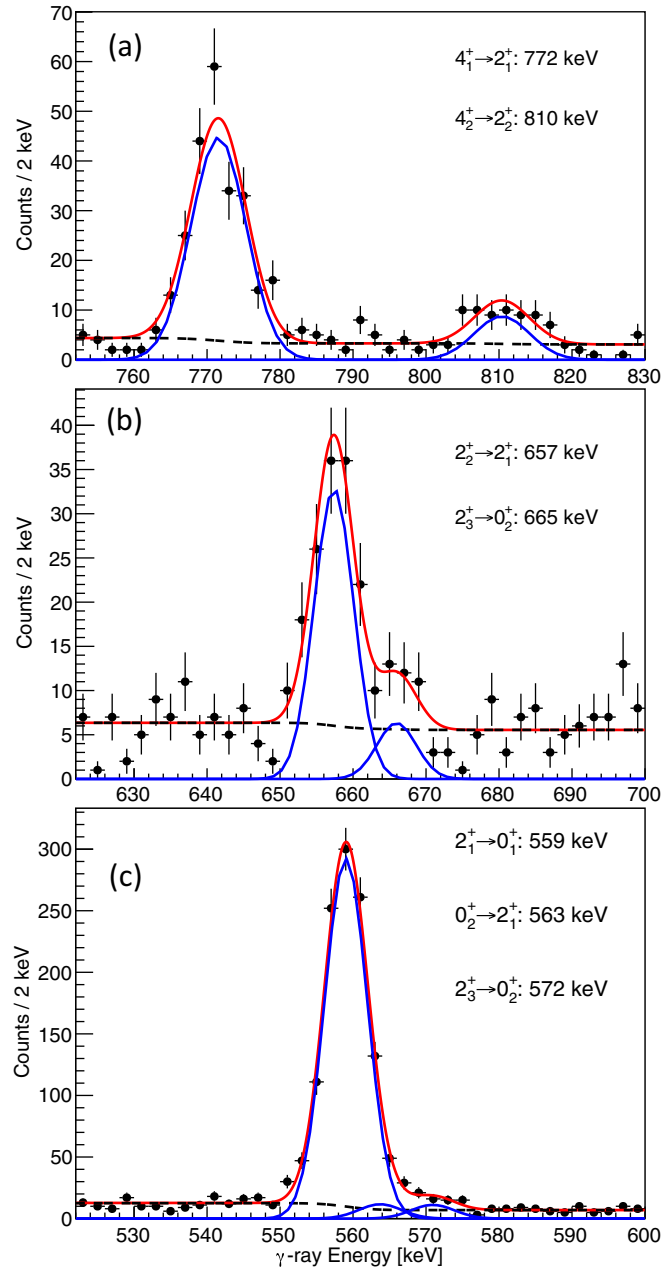

FIG. 4. Doppler-corrected γ rays coincident with the detection of a beamlike particle in the upstream silicon detector. Shown are three cases in which multiplets were observed and fitted with the total fit shown in red (light gray), individual peaks shown in blue (dark gray), and the background shown by a dashed black line.

following the β decay of ^{152}Eu and through comparison with the γ-ray spectrum at backward angles where the components could be extracted through a combined fit of the spectrum at a statistically significant level. The resultant fit is shown in the bottom panel of Fig. 4. The correction factor was then taken as a weighted average of that determined from the two empirical methods. The uncertainty on the values extracted in this method remain dominated by the statistical component.

TABLE I. Experimental values as constraints for the GOSIA calculations presented here. Values taken from Ref. [8] except where indicated. Note that the values from Ref. [18] have been symmetrized for input into GOSIA.

State	Lifetime (ps)	Transition	Mixing ratio (δ)
2_1^+	17.75(29)	$2_2^+ \rightarrow 2_1^+$	5.2(2)
2_2^+	4.91(29)	$2_3^+ \rightarrow 2_2^+$	0.80(55)[a]
4_1^+	2.19(8)	$2_3^+ \rightarrow 2_1^+$	−0.51(5)
2_3^+	1.86(46)[a]	$4_2^+ \rightarrow 4_1^+$	1.7(4)
6_1^+	0.89(10)		
Initial (i)	Final (f_1)	Final (f_2)	BR $[\frac{I(i\rightarrow f_1)}{I(i\rightarrow f_2)}]$
0_2^+	0_1^+	2_1^+	$2.3(4) \times 10^{-4}$
2_2^+	0_1^+	2_1^+	0.59(3)
2_3^+	2_1^+	0_1^+	4.00(23)
2_3^+	2_1^+	0_2^+	3.13(23)
2_3^+	2_1^+	2_2^+	10(2)
2_3^+	2_1^+	4_1^+	33(3)
4_2^+	2_2^+	4_1^+	2.04(23)
4_2^+	2_2^+	2_1^+	20(12)

[a]From Ref. [18].

Coulomb-excitation yields were evaluated using the GOSIA code [17] to determine transition matrix elements. Literature experimental values pertaining to the transitions observed in the present paper were additionally used to constrain the fit and are summarized in Table I. The $E0$ decay of the 0_2^+ state was incorporated through decay to a fictional 1^+ state via a $M1$ decay, constrained by the measured branching ratio. Consistency between the high- and the low-energy data was confirmed by performing an independent GOSIA analysis for each. The final results presented below are from a simultaneous GOSIA analysis with matrix elements minimized to best reproduce both the high- and the low-energy data.

IV. DISCUSSION

The matrix elements resulting from the present analysis are given in Table II. Note that as previously mentioned, literature data were used to constrain a number of matrix elements and so the present values should not be considered as independent of those presented in Table I. $E2$ matrix elements and transition strengths can be used to infer the collective behavior of the nucleus through a number of relations. ^{76}Se has the largest $B(E2; 2_1^+ \rightarrow 0_1^+)$ value, indicating a maximum of collectivity along with the lowest 2_1^+ excitation energy, another indicator of a large degree of collectivity. This is also borne out by the systematics of the spectroscopic quadrupole moments $Q_s(2_1^+)$ with maximum absolute values approximately centered on ^{76}Se, however, this picture is far from complete. Under the assumption of a rigid axial rotor, one can relate $|Q_s(2_1^+)|$ to $B(E2; 2_1^+ \rightarrow 0_1^+)$ by

$$|Q_s(2_1^+)| = \tfrac{2}{7}\sqrt{16\pi B(E2; 2_1^+ \rightarrow 0_1^+)}. \quad (1)$$

The value of $|Q_s(2_1^+)|$ determined in the present paper is only approximately 60% of that determined from the above relation. Coupled with the existence of a low-lying 2_2^+ state

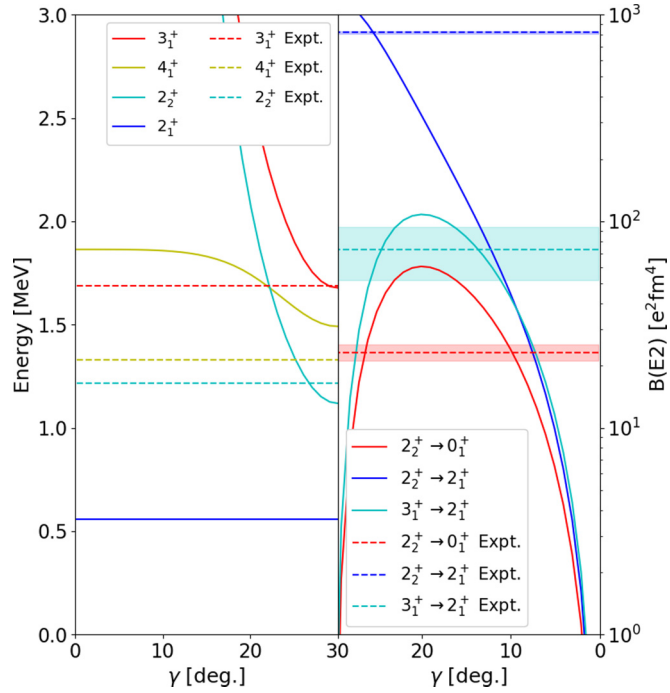

FIG. 5. Level energies (left) and transition strengths (right) expected for the asymmetric rotor, Davydov-Filippov model as a function of the triaxiality parameter γ (solid lines). Experimental values (dashed lines) for ^{76}Se are shown with shaded regions indicating the uncertainties. The experimental data are best described by a triaxiality parameter $\gamma \approx 25^\circ$. Note that the behavior of both energies and transition strengths is symmetric about $\gamma = 30^\circ$. Level energies and transition strengths were normalized to reproduce the experimental 2_1^+ excitation energy and $2_1^+ \rightarrow 0_1^+$ transition strength, respectively.

which can be best described as the bandhead of the so-called γ band, this indicates that a simple symmetric axial rotor description is insufficient to explain the low-lying structure and triaxiality likely plays a significant role in ^{76}Se.

One can compare the level energies and transition strengths of the low-lying states to, for example, the Davydov-Filippov model [22] to estimate the degree of triaxiality in the nuclear system from the assumption of an axially asymmetric rotor. Such an analysis is presented in Fig. 5 for ^{76}Se. Clearly, the level energies and transition strengths are best described by a nucleus approaching maximum triaxiality ($\gamma \approx 25 \rightarrow 30^\circ$). Note that the behavior of level energies and transition strengths in the model is symmetric about $\gamma = 30^\circ$. Using the triaxial rotor model presented in Ref. [23] in which the inertia tensor is treated independently of the electric quadrupole tensor, one can calculate a value for the triaxiality parameter $\gamma \approx 25^\circ$—in good qualitative agreement with the value expected from Fig. 5.

A comparison with geometric models therefore indicates that triaxiality plays a role in the low-lying structure of ^{76}Se, the quality of the present data combined with that in the literature allows for a more rigorous analysis with the presented set of $E2$ matrix elements in Table II sufficient to perform a model-independent analysis of the nuclear shape.

TABLE II. Reduced matrix elements, reduced transition strengths, and quadrupole moments determined in the present paper where available literature values are provided for comparison. Note that, due to the use of experimental observables in the GOSIA minimization, the present results cannot be considered as independent of the literature. Note that $B(E2)\uparrow$ and $B(M1)\uparrow$ values are given.

	This paper		Literature		
	$\langle J_i^\pi \| E2 \| J_f^\pi \rangle$ (*e*b)	$B(E2; J_i^\pi \to J_f^\pi)$ (e^2 fm^4)	$\langle J_i^\pi \| E2 \| J_f^\pi \rangle$ (*e*b)	$B(E2; J_i^\pi \to J_f^\pi)$ (e^2 fm^4)	Reference
$0_1^+ \to 2_1^+$	0.647(5)	$4190(^{60}_{70})$	0.649(7)	4210(68)	[8]
$0_1^+ \to 2_2^+$	0.110(2)	119(5)	$0.108(^{4}_{5})$	116(10)	[8]
$0_1^+ \to 2_3^+$	0.040(1)	16(1)	$0.044(^{10}_{14})$	19(10)	[18]
$2_1^+ \to 0_2^+$	$0.285(^{26}_{27})$	$163(^{30}_{29})$	$0.300(^{64}_{81})$	180(84)	[8]
			$0.47(^{11}_{10})$	$440(^{230}_{168})$	[19]
$2_1^+ \to 2_2^+$	0.640(11)	820(30)	$0.641(^{22}_{23})$	822(57)	[8]
$2_1^+ \to 4_1^+$	$1.108(^{12}_{11})$	2450(50)	$1.105(^{15}_{16})$	2444(69)	[8]
$2_1^+ \to 2_3^+$	$-0.093(^{7}_{6})$	17(2)	$\|0.102(^{14}_{16})\|$	21(6)	[18]
$2_1^+ \to 4_2^+$	$0.039(^{35}_{7})$	$3(^{8}_{1})$	0.04(1)	2.4(17)	[8]
$0_2^+ \to 2_2^+$	$0.182(^{33}_{47})$	$330(^{130}_{150})$	$0.15(^{8}_{18})$	$225(^{304}_{225})$	[19]
$0_2^+ \to 2_3^+$	$0.532(^{21}_{18})$	$2830(^{220}_{190})$	$0.595(^{70}_{90})$	$3540(^{1910}_{960})$	[18]
			$0.59(^{30}_{74})$	$3481(^{4440}_{3481})$	[19]
$2_2^+ \to 4_1^+$	$0.047(^{44}_{29})$	$4.5(^{122}_{38})$	$0.12(^{16}_{12})$	$31(^{131}_{31})$	[19]
$2_2^+ \to 2_3^+$	$0.262(^{67}_{43})$	$140(^{80}_{40})$	$0.19(^{6}_{4})$	$73(^{57}_{27})$	[18]
			$0.30(^{10}_{6})$	$880(^{650}_{325})$	[19]
			<0.022	<4.8	[8]
$2_2^+ \to 4_2^+$	$0.768(^{36}_{37})$	1180(110)	$0.706(^{81}_{91})$	998(241)	[8]
$4_1^+ \to 2_3^+$	$0.418(^{18}_{15})$	$190(^{20}_{10})$	$0.489(^{6}_{7})$	266(74)	[18]
$4_1^+ \to 4_2^+$	$0.733(^{51}_{38})$	$600(^{90}_{60})$	$0.62(^{9}_{11})$	421(134)	[8]
$4_1^+ \to 6_1^+$	$1.390(^{64}_{58})$	$2050(^{200}_{180})$	$1.3(^{8}_{7})$	1880(220)	[8]
	$\langle J_i^\pi \| M1 \| J_f^\pi \rangle$ (μ_n)	$B(M1; J_i^\pi \to J_f^\pi)$ (μ_N^2)	$\langle J_i^\pi \| M1 \| J_f^\pi \rangle$ (μ_n)	$B(M1; J_i^\pi \to J_f^\pi)$ (μ_N^2)	Reference
$2_1^+ \to 2_2^+$	0.067(3)	$9.1(^{0.8}_{0.7}) \times 10^{-4}$	0.068(3)	$9.2(9) \times 10^{-4}$	[8]
$2_1^+ \to 2_3^+$	$0.186(^{4}_{5})$	$7.0(3) \times 10^{-3}$	0.16(2)	$5(1) \times 10^{-3}$	[18]
$2_2^+ \to 2_3^+$	$0.168(^{4}_{2})$	$6(^{3}_{1}) \times 10^{-3}$	$0.14(^{4}_{3})$	$4(2) \times 10^{-3}$	[18]
$4_1^+ \to 4_2^+$	$0.158(^{5}_{3})$	$3(^{2}_{1}) \times 10^{-3}$	$0.13(^{4}_{3})$	$2(1) \times 10^{-3}$	[18]
	$\langle J_i^\pi \| E2 \| J_i^\pi \rangle$ (*e*b)	$Q_s(J^\pi)$ (*e*b)	$\langle J_i^\pi \| E2 \| J_i^\pi \rangle$ (*e*b)	$Q_s(J^\pi)$ (*e*b)	Reference
$2_1^+ \to 2_1^+$	$-0.463(^{52}_{53})$	−0.35(4)	−0.449(92)	−0.34(7)	[20]
			−0.396(106)	−0.30(5)	[21] via [8]
			−0.45(7)	−0.34(5)	[19]
$2_2^+ \to 2_2^+$	$0.245(^{57}_{60})$	0.19(4)	$0.24(^{6}_{8})$	$0.18(^{5}_{6})$	[19]
$4_1^+ \to 4_1^+$	$-0.387(^{55}_{53})$	−0.29(4)	$-0.36(^{24}_{14})$	$-0.27(^{18}_{11})$	[19]

The electric multipole transition operator is a spherical tensor allowing for rotationally invariant zero-coupled products to be constructed which can themselves be linked to the intrinsic deformation of the nucleus [24,25]. The two invariant products discussed here relate to the quadrupole deformation parameters of the nucleus. The first quadrupole invariant to be constructed Q corresponds to the overall deformation of the nucleus in analogy to the β parameter of the Bohr Hamiltonian but relating to the distribution of charge rather than mass. By expanding over all intermediate states using the Wigner $6j$ symbol, one can write

$$\frac{\langle Q^2 \rangle}{\sqrt{5}} = \frac{(-1)^{2I_i}}{\sqrt{(2I_i+1)}} \sum_t \langle i||E2||t\rangle\langle t||E2||i\rangle \begin{Bmatrix} 2 & 2 & 0 \\ I_i & I_i & I_t \end{Bmatrix}. \tag{2}$$

The second invariant to be considered δ relates to the degree of triaxiality in the intrinsic frame, in analogy to Bohr's γ parameter but again relating to the charge distribution. This is a higher-order invariant, which, expanding again over all intermediate states, yields

$$\sqrt{\frac{2}{35}}\langle Q^3 \cos(3\delta)\rangle = \mp \frac{1}{(2I_i+1)} \sum_{t,u} \langle i||E2||u\rangle\langle u||E2||t\rangle\langle t||E2||i\rangle \begin{Bmatrix} 2 & 2 & 2 \\ I_i & I_t & I_u \end{Bmatrix}, \tag{3}$$

where a negative sign corresponds to integer spins and a positive sign corresponds to a half-integer. Here, we further

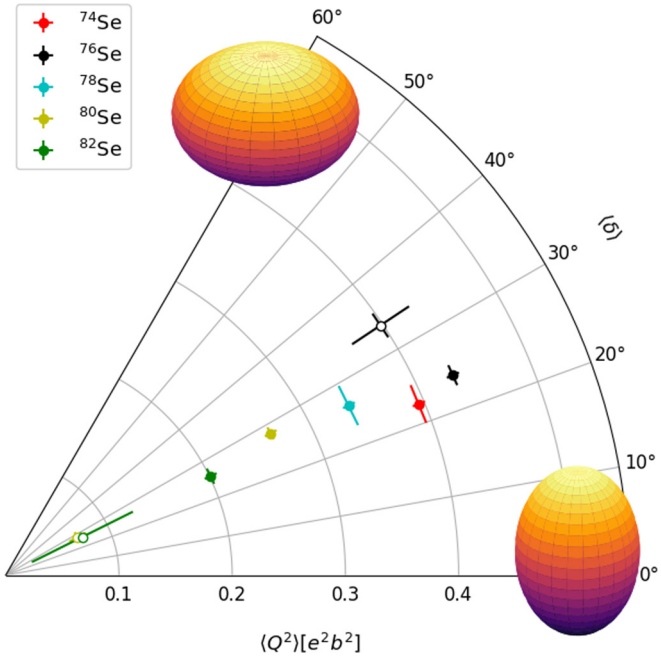

FIG. 6. $\langle Q^2\rangle$ and $\langle\delta\rangle$ calculated using the invariant values described in Eqs. (2) and (3) for the 0_1^+ (solid symbols) and 0_2^+ (open symbols) states in stable selenium isotopes. ^{76}Se values were deduced from the matrix elements determined in the present paper, whereas ^{74,78,80,82}Se were determined from data presented in Refs. [8,19,26–28]. Note that, as discussed in the text, uncertainties correspond to matrix-element uncertainties only and do not incorporate any uncertainties in convergence.

assume that

$$\langle\cos(3\delta)\rangle \approx \frac{\langle Q^3\cos(3\delta)\rangle}{(\langle Q^2\rangle)^{3/2}}. \tag{4}$$

Invariants were thereby determined for stable selenium isotopes and the $\langle\delta\rangle$ and $\langle Q^2\rangle$ parameters are presented in Fig. 6 in $(\langle Q^2\rangle, \langle\delta\rangle)$ space, in analogy to the (β, γ) space often used to represent the Bohr deformation parameters. The use of the present data to determine the shape invariants rather than that available in the literature results in a 30% reduced uncertainty in the determination of $\langle\cos(3\delta)\rangle$ for the 0_1^+ state. For the 0_2^+ state, a better than 60% improvement in precision is found for both $\langle Q^2\rangle$ and $\langle\cos(3\delta)\rangle$. Note that $\langle 2_3^+ | E2 | 2_3^+\rangle$ has not been determined in any stable selenium isotope. The contribution of this matrix element to the ground-state $\langle\cos(3\delta)\rangle$ values is expected to be small due to $\langle 0_1^+ | E2 | 2_3^+\rangle$ being small in all cases where it has been measured. In the case of the 0_2^+ state, however, the contribution can be significant due to the larger magnitude of the $\langle 0_2^+ | E2 | 2_3^+\rangle$ matrix element. The $\langle\delta\rangle$ values for the 0_2^+ states presented in Fig. 6 (open symbols) might, therefore, not be converged.

The $\langle\cos(3\delta)\rangle$ parameter, as previously stated, relates to the degree of triaxiality of the state in question—in this case, the 0_1^+ and 0_2^+ states. A value of $\delta = 60^\circ$ [$\langle\cos(3\delta)\rangle = -1$] corresponds to an axially symmetric oblate shape, and a value of $\delta = 0^\circ$ [$\langle\cos(3\delta)\rangle = 1$] corresponds to an axially symmetric prolate shape. The $\langle Q\rangle$ parameter, meanwhile, relates to the absolute magnitude of deformation. From Fig. 6, therefore, it is clear that, although the absolute degree of deformation in selenium isotopes increases from $A = 82 \rightarrow 74$, the nuclear shapes never stabilize into an axially symmetric rotor. Instead, the nuclei exhibit a significant—albeit not maximal—degree of triaxiality. Note that the presented invariant values are only sensitive to the average degree of triaxiality and not to the degree of rigidity of the triaxial deformation. Higher-order invariant quantities than those expressed in Eqs. (2) and (3) can also be constructed to quantify the rigidity of the Q and δ values but require an even larger collection of matrix elements than presented here.

TABLE III. Experimental $B(E2)$ transition strengths and spectroscopic quadrupole moments for ^{76}Se compared to those calculated using the configuration interaction in the $jj44$ model space with two different interactions using an isoscalar effective charge: $e^\pi = 1.8$, $e^\nu = 0.8$. Experimental values from this paper (see Table II). See the text for details.

$B(E2; I \rightarrow F)$ (e^2 fm^4)	Expt.	$jj44b$	JUN45
$2_1^+ \rightarrow 0_1^+$	838 (14)	788	678
$2_2^+ \rightarrow 0_1^+$	23.8 (10)	2.4	44.2
$2_2^+ \rightarrow 2_1^+$	820 (30)	1073	273
$Q_s(I)$ (eb)			
2_1^+	−0.35 (4)	+0.08	+0.49
2_2^+	+0.19 (4)	−0.09	−0.42
4_1^+	−0.29 (4)	+0.27	+0.27

A. Shell-model calculations

A microscopic comparison to the present data can be made through comparison with configuration interaction (CI) calculations in the so-called $jj44$ model space, which is made up of the $0f_{5/2}$, $1p_{3/2}$, $1p_{1/2}$, and $0g_{9/2}$ orbitals for both protons and neutrons. Calculations were performed using the shell-model code NUSHELLX [29] using both the JUN45 [6] and the $jj44b$ (see Appendix A in Ref. [7]) Hamiltonians with an isoscalar effective charge of $e^\pi + e^\nu = 2.6$. These calculations were previously presented more broadly for low-lying states in ^{76}Se [18] and ^{76}Ge [7] with a detailed description of the calculations presented in Appendix A of the latter reference. Here, we will focus on the transition strengths most pertinent to the present results.

Table III shows transition strengths for the lowest-lying 2^+ states and quadrupole moments for the 2_1^+, 2_2^+, and 4_1^+ states determined both experimentally and in the CI calculations. The $2_1^+ \rightarrow 0_1^+$ transition strength is relatively well reproduced with the $jj44b$ Hamiltonian providing the best agreement. Similarly, the $jj44b$ interaction provides the best reproduction of the $2_2^+ \rightarrow 2_1^+$ transition strength, albeit overestimating the relative strength as compared to the $2_1^+ \rightarrow 0_1^+$ transition. The $2_2^+ \rightarrow 0_1^+$ strength is underpredicted by the $jj44b$ interaction, however, with the JUN45 providing the better agreement. If one were to interpret these results in the context of the Davydov-Filippov model (Fig. 5), the $jj44b$ calculations would appear to predict near-maximal triaxiality, whereas the

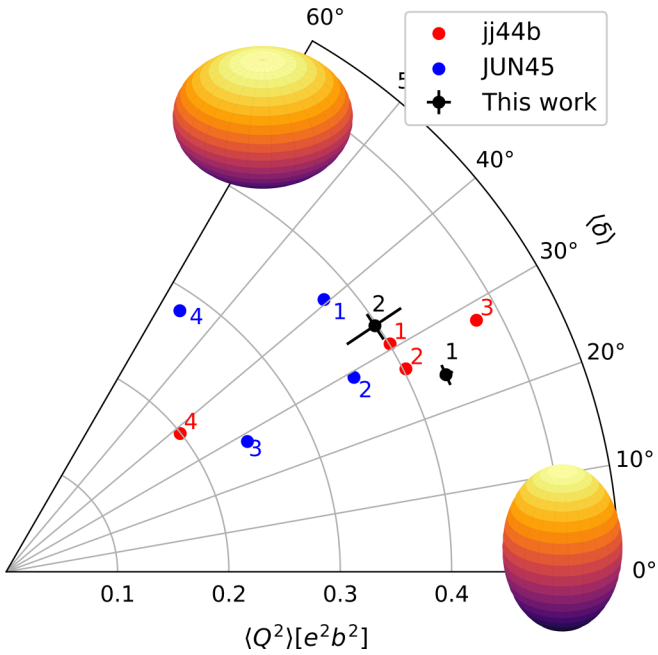

FIG. 7. $\langle Q^2 \rangle$ and $\langle \delta \rangle$ calculated using the invariant values described in Eqs. (2) and (3). Present experimental results for ^{76}Se (black points) along with values determined from shell-model calculations performed using the $jj44b$ and JUN45 interactions. Numbered points indicate the energy ordering of the 0^+ states (i.e., 1 corresponds to 0^+_1, 2 to 0^+_2, etc.). Uncertainties correspond to matrix-element uncertainties only and do not incorporate any uncertainties in convergence. See the text for details.

calculations using the JUN45 Hamiltonian predict a rather less triaxial structure—albeit not axially symmetric as evidenced by non-negligible $2^+_2 \rightarrow 2^+_1$ strength. This interpretation is strengthened by comparison of the quadrupole moments with the JUN45 calculations resulting in larger absolute values, whereas the $jj44b$ values are considerably smaller. Investigation of the quadrupole moments appears to indicate a discrepancy between experiment and both calculations, however, with predictions of a positive quadrupole moment—indicative of an oblate deformation—being in conflict with the experimentally determined negative value (prolate).

To investigate further, the rotational invariants in Eqs. (2) and (3) were constructed from the calculated matrix elements. The 2^+ states up to 2^+_5 were included in the determination of the invariants, increasing confidence in convergence. As before, we present these calculated values in Fig. 7 in $(\langle Q^2 \rangle, \langle \delta \rangle)$ space. $\langle Q^2 \rangle$ and $\langle \delta \rangle$ values were calculated for 0^+_{1-4} and are compared to those calculated from experimentally determined matrix elements for the 0^+_1 and 0^+_2 states in ^{76}Se. The $jj44b$ calculations appear to provide the best description of the two lowest-lying 0^+ states, albeit with the ground state exhibiting a modest dominance by oblate deformation as compared to prolate deformation in the experimental data. Nonetheless, the agreement is considerably better than might be assumed if one were to merely compare the signs and magnitudes of the $Q_s(2^+_1)$ values. Due to the more comprehensive collection of $E2$ matrix elements determined from the CI calculations, higher-order invariants can be constructed to assess the degree of rigidity in $\langle Q^2 \rangle$ and $\cos(3\delta)$. It is found that the $jj44b$ calculations correspond to a very δ-soft structure, whereas the JUN45 calculations result in a more rigid configuration.

V. CONCLUSIONS

A low-energy Coulomb excitation measurement of ^{76}Se was performed using the JANUS setup at the ReA3 facility of the NSCL. A number of electric quadrupole matrix elements were extracted using the GOSIA code with good agreement between the present results and those in the literature where available. The spectroscopic quadrupole moment of the first 2^+ state was measured at improved precision, remaining consistent with a prolate deformation. An analysis of rotational invariants with the new higher-precision data was performed to probe the intrinsic structure of the bands built upon the 0^+_1 and 0^+_2 states. The ground state is found to exhibit significant triaxiality, albeit with a dominant prolate component. The 0^+_2 state is also found to be consistent with a triaxial deformation; however, the present measurement was unable to determine the diagonal matrix element of the 2^+_3 state which, due to the large magnitude of $\langle 0^+_2 | E2 | 2^+_3 \rangle$, will likely contribute significantly to the triaxial invariant of the 0^+_2 state.

Comparison with configuration interaction calculations were performed. The present result highlights the need for a detailed analysis of theoretical results before comparison with experiment. A first-order analysis might imply that the CI calculations failed dramatically to reproduce the experimental data due to the differing signs of the spectroscopic quadrupole moments. The construction of invariants using the calculated $E2$ matrix elements, however, demonstrate that the calculations, in fact, reproduce the structure relatively well as shown in Table III. A more comprehensive set of $E2$ matrix elements for the even-even selenium isotopes might allow further investigation of the role of triaxiality in the excited 0^+ states, which cannot be conclusively determined in the present paper.

Previous studies into the effects of deformation on $0\nu2\beta$ matrix elements have focused on axial shapes (e.g., Ref. [5]). The present result, coupled to the low-lying structure of ^{76}Ge, which also points towards triaxiality, indicates that future investigations should take nonaxial shapes into account.

Figure 1 was created using the SciDraw scientific figure preparation system [30].

ACKNOWLEDGMENTS

The authors thank the ReA3 beam delivery group at the NSCL for the high-quality beam of ^{76}Se. The authors acknowledge discussions with S. W. Yates. Work at LLNL was performed under Contract No. DE-AC52-07NA27344. This work was supported, in part, by the National Science Foundation under Contract No. PHY-1565546 (NSCL), by the US Department of Energy, Office of Nuclear Physics under Grant No. DE-FG02-08ER41556 (NSCL), and by the DOE National Nuclear Security Administration through the Nuclear Science and Security Consortium under Award No. DE-NA0003180.

[1] G. H. Bhat, W. A. Dar, J. A. Sheikh, and Y. Sun, Phys. Rev. C **89**, 014328 (2014).

[2] A. D. Ayangeakaa, R. V. F. Janssens, C. Y. Wu, J. M. Allmond, J. L. Wood, S. Zhu, M. Albers, S. Almaraz-Calderon, B. Bucher, M. P. Carpenter, C. J. Chiara, D. Cline, H. L. Crawford, H. M. David, J. Harker, A. B. Hayes, C. R. Hoffman, B. P. Kay, K. Kolos, A. Korichi, T. Lauritsen, A. O. Macchiavelli, A. Richard, D. Seweryniak, and A. Wiens, Phys. Lett. B **754**, 254 (2016).

[3] The GERDA Collaboration, Nature (London) 544, 47 (2017).

[4] N. Abgrall *et al.*, Adv. High Energy Phys. **2014**, 1 (2014).

[5] J. M. Yao, L. S. Song, K. Hagino, P. Ring, and J. Meng, Phys. Rev. C **91**, 024316 (2015).

[6] M. Honma, T. Otsuka, T. Mizusaki, and M. Hjorth-Jensen, Phys. Rev. C **80**, 064323 (2009).

[7] S. Mukhopadhyay, B. P. Crider, B. A. Brown, S. F. Ashley, A. Chakraborty, A. Kumar, M. T. McEllistrem, E. E. Peters, F. M. Prados-Estévez, and S. W. Yates, Phys. Rev. C **95**, 014327 (2017).

[8] NNDC, "Evaluated Nuclear Structure Data File (ENSDF)".

[9] A. Villari, G. Bollen, M. Ikegami, S. Lidia, R. Shane, Q. Zhao, D. Alt, D. Crisp, S. Krause, A. Lapierre, D. Morrissey, S. Nash, R. Rencsok, R. Ringle, S. Schwarz, C. Sumithrarachchi, and S. Williams, in *Proceedings of International Particle Accelerator Conference (IPAC'16), Busan, Korea, 2016* (Pohang Accelerator Laboratory, Gyeongbuk, Republic of Korea, 2016), pp. 1287–1290.

[10] A. Gade and B. M. Sherrill, Phys. Scr. **91**, 053003 (2016).

[11] A. Lapierre, S. Schwarz, T. M. Baumann, K. Cooper, K. Kittimanapun, A. J. Rodriguez, C. Sumithrarachchi, S. J. Williams, W. Wittmer, D. Leitner, and G. Bollen, Rev. Sci. Instrum. **85**, 02B701 (2014).

[12] E. Lunderberg, J. Belarge, P. C. Bender, B. Bucher, D. Cline, B. Elman, A. Gade, S. N. Liddick, B. Longfellow, C. Prokop, D. Weisshaar, and C. Y. Wu, Nucl. Instrum. Methods Phys. Res., Sect. A **885**, 30 (2018).

[13] W. Mueller, J. Church, T. Glasmacher, D. Gutknecht, G. Hackman, P. Hansen, Z. Hu, K. Miller, and P. Quirin, Nucl. Instrum. Methods Phys. Res., Sect. A **466**, 492 (2001).

[14] P. C. Bender, https://github.com/pcbend/GRUTinizer/

[15] R. Brun and F. Rademakers, Nucl. Instrum. Methods Phys. Res., Sect. A **389**, 81 (1997).

[16] J. Henderson, C. Y. Wu, J. Ash, P. C. Bender, B. Elman, A. Gade, M. Grinder, H. Iwasaki, E. Kwan, B. Longfellow, T. Mijatovíc, D. Rhodes, M. Spieker, and D. Weisshaar, Phys. Rev. Lett. **121**, 082502 (2018).

[17] T. Czosnyka, D. Cline, and C. Y. Wu, Bull. Am. Phys. Soc. **28**, 745 (1983).

[18] S. Mukhopadhyay, B. P. Crider, B. A. Brown, A. Chakraborty, A. Kumar, M. T. McEllistrem, E. E. Peters, F. M. Prados-Estévez, and S. W. Yates, Phys. Rev. C **99**, 014313 (2019).

[19] A. Kavka, C. Fahlander, A. Backlin, D. Cline, T. Czosnyka, R. Diamond, D. Disdier, W. Kernan, L. Kraus, I. Linck, N. Schulz, J. Srebrny, F. Stephens, L. Svensson, B. Varnestig, E. Vogt, and C. Wu, Nucl. Phys. **A593**, 177 (1995).

[20] R. Lecomte, P. Paradis, J. Barrette, M. Barrette, G. Lamoureux, and S. Monaro, Nucl. Phys. **A284**, 123 (1977).

[21] P. B. Vold, D. Cline, J. Sprinkle, and R. Scharenberg, Bull. Am. Phys. Soc. **21**, 581 (1976).

[22] A. Davydov and G. Filippov, Nucl. Phys. **8**, 237 (1958).

[23] J. L. Wood, A.-M. Oros-Peusquens, R. Zaballa, J. M. Allmond, and W. D. Kulp, Phys. Rev. C **70**, 024308 (2004).

[24] K. Kumar, Phys. Rev. Lett. **28**, 249 (1972).

[25] D. Cline, Annu. Rev. Nucl. Part. Sci. **36**, 683 (1986).

[26] R. Lecomte, S. Landsberger, P. Paradis, and S. Monaro, Phys. Rev. C **18**, 2801 (1978).

[27] J. Barrette, M. Barrette, G. Lamoureux, S. Monaro, and S. Markiza, Nucl. Phys. **A235**, 154 (1974).

[28] T. Hayakawa, Y. Toh, M. Oshima, A. Osa, M. Koizumi, Y. Hatsukawa, Y. Utsuno, J. Katakura, M. Matsuda, T. Morikawa, M. Sugawara, H. Kusakari, and T. Czosnyka, Phys. Rev. C **67**, 064310 (2003).

[29] B. A. Brown and W. D. M. Rae, Nucl. Data Sheets **120**, 115 (2014).

[30] M. A. Caprio, Comput. Phys. Commun. **171**, 107 (2005).